JOURNAL OF SOLID STATE CHEMISTRY **129,** 271–276 (1997)
ARTICLE NO. SC967241

A Wide Angle X-Ray Scattering (WAXS) Study of Nonstoichiometric Nickel Manganite Spinels $NiMn_2\square_{3\delta/4}O_{4+\delta}$

Christel Laberty,* Marc Verelst,[†,1] Pierre Lecante,[†] Pierre Alphonse,*[,1] Alain Mosset,[†] and Abel Rousset*

*Laboratoire de Chimie des Matériaux Inorganiques, Université Paul Sabatier, 118 route de Narbonne, 31062 Toulouse Cedex, France; and
[†]Centre d'Elaboration de Matériaux et d'Etudes Structurales, UP 8011, B.P. 4347, 29 rue Jeanne Marvig, 31055 Toulouse Cedex, France

Received November 18, 1996; accepted November 21, 1996

WAXS study of highly divided oxides obtained by low temperature decomposition of mixed oxalates $NiMn_2(C_2O_4)_3\cdot nH_2O$ in air at low temperatures (573 and 623 K) shows that oxalate decomposition leads probably directly to the spinel structure $NiMn_2\square_{3\delta/4}O_{4+\delta}$ with a very high content of cation vacancies essentially located in tetrahedral sites. Thermogravimetric analyses confirm that these oxides have a great nonstoichiometry proportion; the higher value ($\delta \approx 0.9$) is observed for the compound synthesized at 573 K.

INTRODUCTION

Nickel manganites are usually prepared by thermal decomposition of mixed manganese–nickel oxalate $Ni_{x/3}Mn_{3-x/3}C_2O_4\cdot nH_2O$ at 1173 K in air. These oxides have a low specific surface area ($1\,m^2\cdot g^{-1}$) and are stoichiometric (1, 2). The thermal decomposition of manganese-nickel oxalate at low temperature ($T < 623$ K) (3–5) has recently been investigated and it was found that it gives cation deficient spinels $Ni_xMn_{3-x}\square_{3\delta/4}O_{4+\delta}$. These oxides are finely divided materials since their BET specific surface area is close to $100\,m^2\,g^{-1}$ and the average diameter of their crystallites is about 10 nm (6). The proportion of cation deficiency δ has been evaluated by TGA studies under controlled atmosphere. It varies with nickel content; a maximum of 0.9 is found for $x = 0.4$ (6). This large nonstoichiometry can be correlated with the high reactivity of these compounds toward molecules such as O_2, CO, or hydrocarbons.

Generally stoichiometric mixed manganites $A_xMn_{3-x}O_4$ (A = Mg, Mn, Co, Zn) are normal spinels and have the cation distribution: $A_x^{2+}Mn_{1-x}^{2+}[Mn^{3+}Mn^{3+}]O_4^{2-}$. Because of the strong prefeence of the Ni^{2+} cation for octahedral sites, nickel manganites are inverse spinels with the cation arrangement $Mn^{2+}[Ni_x^{2+}Mn_x^{4+}Mn_{2-2x}^{3+}]O_4^{2-}$. Occupation of the octahedral sites by Ni^{2+} induces $Mn^{3+/4+}$ redox couples on the same lattice sites. These couples are the cause of the good electrical conductivity of nickel manganites (normal manganite spinels are all insulators) and these materials have been widely studied for their application as thermistor ceramics (7–9). For $x = 1$, the cation distribution would be $Mn^{2+}[Ni^{2+}Mn^{4+}]O_4^{2-}$, but this arrangement does not account for the good conductivity of this oxide, which implies that a part of Ni^{2+} cations must be in tetrahedral sites. Moreover some authors have proposed, from neutron diffraction studies, that tetrahedral sites contain also a small proportion of Mn^{3+} cations (10). Thus, the determination of cation distribution of stoichiometric nickel manganites is not an easy task and although many works have been published, this subject is not beyond controversy. New difficulties arise with the cation deficient nickel manganites because they are badly crystallized, and getting structural information from amorphous or simply poorly crystallized compounds is not easy since few methods provide accurate structural information in that case. The EXAFS technique, which gives valuable structural information, is now widely used but EXAFS information is restricted to the first or second coordination sphere around a central atom. Another possible technique for obtaining significant information on the structural architecture of amorphous materials is WAXS (wide angle X-ray scattering). This technique is used to investigate quite different materials such as organometallic polymers (11), amorphous semiconductors (12), and binary oxides (13). Provided careful data collection and reduction procedures are performed, WAXS can be used as an almost routine technique permitting useful experimentation on short and medium range order up to 20 Å.

We report here WAXS and TGA studies of two nonstoichiometric oxides obtained from low temperature decomposition of mixed oxalates $NiMn_2(C_2O_4)_3\cdot nH_2O$.

[1] To whom correspondence should be addressed.

0022-4596/97 $25.00

EXPERIMENTAL SECTION

Materials. The mixed oxalate $NiMn_2(C_2O_4)_3 \cdot nH_2O$ was precipitated by adding ammonium oxalate to a solution of nickel nitrate (II) and manganese nitrate (II) at room temperature. After one hour, the mixture was filtered, washed several times with deionized water and dried at 330 K in air.

TGA study. Thermal analyses were carried out in a vertical plug flow reactor under a controlled atmosphere. The reactions were followed both by thermogravimetric analysis (Cahn D200 microbalance—accuracy 10^{-6} g) and by mass spectrometry (Leybold Inficon Transpector H200M) analysis of gas flow. Oxalates were decomposed under a 20/80 mixture of O_2/N_2 (with $H_2O < 10$ ppm) by heating them at 573 K (compound MN573) or 623 K (compound MN623) for 6 h, with a heating rate of $2.5\ K \cdot min^{-1}$. Mixed oxides were obtained by heating under Ar until 1000 K with a heating rate of $10\ K \cdot min^{-1}$.

The chemical composition of the oxalates and oxides were determined by atomic absorption spectrometry.

WAXS study. Amorphous powder of MN573 and MN623 was sealed in a Lindeman capillary ($\varnothing = 1.5$ mm). The diffusion spectrum scattered by the sample irradiated with graphite-monochromatized molybdenum $K\alpha$ radiation for MN573 (silver $K\alpha$ radiation for MN623) was obtained using a CAD4 (MN573) or a LASIP diffractometer (MN623).[2] At 21°C 469 intensities in the range $1.5° < \theta < 65°$ (MN573), and 580 intensities in the range $0.8° < \theta < 65°$ (MN623) corresponding to equidistant s points ($s = 4\pi(\sin\theta/\lambda)$; $\Delta s = 0.035365$ (MN573), 0.03494 (MN623)) were collected. Just afterwards measurements of air and Lindeman capillary diffusion were done exactly in the same conditions. The raw sample scattered intensity (sample + air + capillary) was corrected for air and capillary contribution and polarization effect. A sample absorption correction was fitted considering that the corrected scattered intensity divided by the independent intensity must oscillate around a constant value (the normalization factor). The exact value of the normalization factor was determined from the Norman and Krogh-Moe methods (14). The atomic scattering factors were taken from Cromer and Waber (15). The experimental reduced radial distribution function (RDF), which show the distribution of the interatomic distances, were calculated as in Ref. (11). The theoretical reduced RDF is calculated for structural models by Fourier transform using the Debye theoretical intensity formula (16).

[2] Laboratory-built 2-axis diffractometer optimized for WAXS: silver radiation, very low air background, continuous rotation of the sample during measurement.

RESULTS

TGA study. As shown by previous studies, the thermal decomposition of the mixed oxalates is a two-stage process (Fig. 1). The first stage corresponds to the dehydration,

$$Ni_{1/3}Mn_{2/3}C_2O_4 \cdot nH_2O \rightarrow Ni_{1/3}Mn_{2/3}C_2O_4 + nH_2O, \quad [1]$$

and the second one to the oxalate decomposition itself,

$$Ni_{1/3}Mn_{2/3}C_2O_4 + \tfrac{2}{3}O_2 \rightarrow \tfrac{1}{3}NiMn_2O_4 + 2CO_2\,. \quad [2]$$

If Δm_{dehy} and Δm are respectively the mass loss (%) for the dehydration step and the total mass loss of the two reactions, n, the number of H_2O molecules per oxalate formula unit, can be computed from Δm_{dehy} according to:

$$n = \frac{\text{mass of } H_2O / M_{H_2O}}{\text{number of oxalate mole}} = \frac{\text{mass of } H_2O / M_{H_2O}}{(m_{init} - \text{mass of } H_2O)/M_{\text{anhydrous oxa}}}, \quad [3]$$

where m_{init} is the initial mass of oxalate and "M_x" means "atomic or molecular mass of atom or molecule x".

Since mass of $H_2O = m_{init}\,\Delta m_{dehy}/100$ we obtain:

$$n = \frac{\Delta m_{dehy} M_{\text{anhydrous oxa}}}{M_{H_2O}(100 - \Delta m_{dehy})} \quad \text{with} \quad M_{\text{anhydrous oxa}} = \tfrac{2}{3}M_{Mn} + \tfrac{1}{3}M_{Ni} + M_{C_2O_4}\,. \quad [4]$$

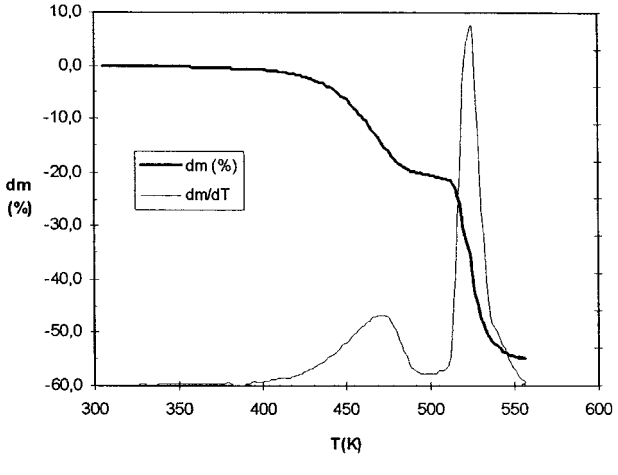

FIG. 1. Thermogravimetric analysis of mixed manganese–nickel oxalate decomposition (atmosphere O_2/N_2, 20/80, heating rate, $2\ K \cdot min^{-1}$).

On the other hand, from total mass loss of the reaction Δm, it is possible to compute the nonstoichiometry proportion, δ. Since the global equation of mixed oxalate decomposition leading to nonstoichiometric oxide $Ni_xMn_{3-x}\square_{3\delta/4}O_{4+\delta}$ is

$$NiMn_2(C_2O_4)\cdot 3nH_2O + \frac{4+\delta}{2}O_2 \rightarrow NiMn_2\square_{3\delta/4}O_{4+\delta} + 6CO_2 + 3nH_2O, \quad [5]$$

the mass loss (in percent) will be

$$\Delta m = 100\left[1 - \frac{M_{Ni} + 2M_{Mn} + (4+\delta)M_O}{M_{Ni} + 2M_{Mn} + 3(M_{C_2O_4} + nM_{H_2O})}\right]. \quad [6]$$

Knowing n, from Eq. [4] we can deduce δ:

$$\delta = \left[3\left(1 - \frac{\Delta m}{100}\right)(M_{C_2O_4} + nM_{H_2O}) - \frac{\Delta m}{100}(M_{Ni} + 2M_{Mn})\right] \Big/ M_O - 4. \quad [7]$$

Values of Δm_{dehy}, Δm, n, and δ corresponding to the oxides MN573 and MN623 are reported in Table 1.

When the nonstoichiometric oxide is heated under a nonoxidizing atmosphere (Ar), Fig. 2 shows that a subsequent mass loss can be observed. The DTG curve shows that this mass loss occurs in several steps. On the other hand, XRD analysis of the residue remaining after the heating process shows the presence of NiO, which indicate that demixing of the oxide has occurred. However, heating MN623 under argon below 800 K does not lead to the formation of nickel oxide. Hence, it seems that demixing occurs only on heating above 800 K, which precisely correspond to a change of slope on the DTG curve.

By assuming that the stoichiometric oxide is formed at this temperature, it becomes possible to compute the value of δ from these experiments. The reduction of oxide can be written as

$$NiMn_2\square_{3\delta/4}O_{4+\delta} \rightarrow NiMn_2O_4 + \frac{\delta}{2}O_2. \quad [8]$$

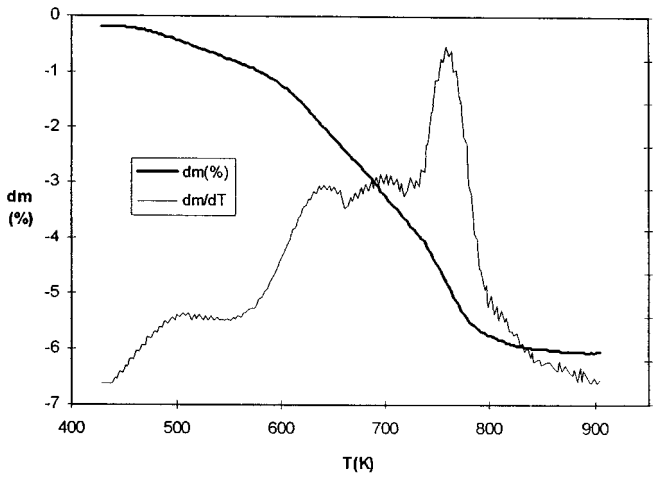

FIG. 2. Thermogravimetric analysis of MN573 (atmosphere, Ar; heating rate, 10 K · min^{-1}).

The mass loss (in percent) will be

$$\Delta m_{800} = 100\left[1 - \frac{M_{Ni} + 2M_{Mn} + 4M_O}{M_{Ni} + 2M_{Mn} + (4+\delta)M_O}\right]. \quad [9]$$

From Eq. [9] we can deduce δ:

$$\delta = \frac{\Delta m_{800}[M_{Ni} + 2M_{Mn} + 4M_O]}{M_O(100 - \Delta m_{800})}. \quad [10]$$

Values of Δm_{800} and δ computed from this equation are reported in Table 2.

Although slightly greater, these values are in excellent agreement with those obtained from oxalate decomposition.

WAXS study. Figure 3 compares the experimental reduced RDF (a) of MN573 with some theoretical ones calculated for different structural models. The first one (b) is a stoichiometric $NiMn_2O_4$ model built up from eight spinel unit cells (two along each axis) with structural parameters taken from the neutron diffraction study published by Gillot *et al.* (10). Clearly MN573 shows a reduced RDF which is quite similar to the $NiMn_2O_4$ one. This reveals that amorphous nickel manganite, decomposed at 573 K, has a structural arrangement based on the $NiMn_2O_4$ spinel

TABLE 1
Values of Δm_{dehy}, Δm, n, and δ Corresponding to the Oxides MN573 and MN623

Oxide	Δm_{dehy}	Δm	n	δ
MN573	20.53	54.9	2.07	0.81
MN623	20.65	55.4	2.08	0.66

TABLE 2
Values of Δm_{800}, and δ Computed from Eq. [10]

Oxide	Δm_{800}	δ
MN573	5.56	0.85
MN623	4.57	0.70

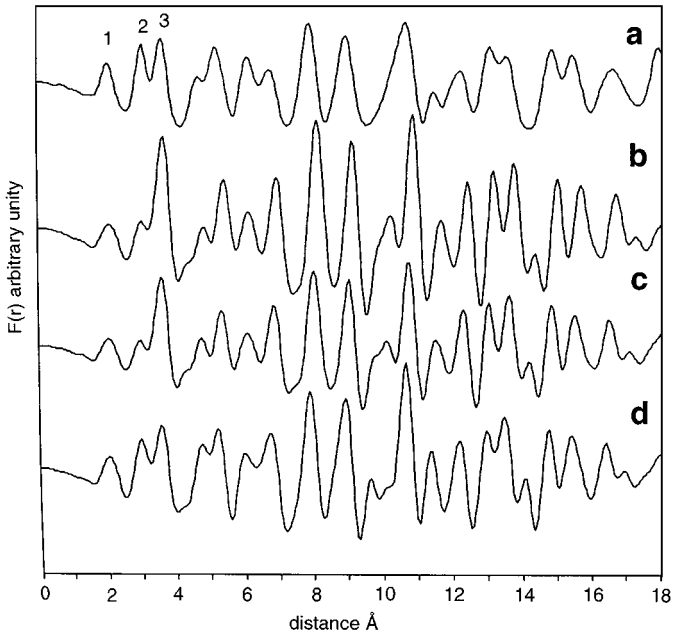

FIG. 3. Experimental reduced RDF for MN573 (a) compared to theoretical reduced RDF calculated for spinel models of: (b) stoichiometric $NiMn_2O_4$ ($a = 8.40$ Å, UO = 0.388); (c) $Ni^{2+}_{0.7}\square_{0.3}[Ni^{2+}_{0.1}Mn^{4+}_{1.6}\square_{0.3}]O_4$ ($a = 8.32$ Å, UO = 0.388); (d) $Ni^{2+}_{0.4}\square_{0.6}[Ni^{2+}_{0.4}Mn^{4+}_{1.6}]O_4$ ($a = 8.32$ Å, UO = 0.388).

structure. However a sensible discrepancy can be noticed. Each peak on the experimental reduced RDF is present on the theoretical reduced RDF, but the peaks on the experimental reduced RDF are systematically shifted toward shorter distances compared to the model. This is all the more noticeable as the distance is larger and it results simply from a cell parameter lower for MN573 than for stoichiometric $NiMn_2O_4$.

More interesting are the second and third peak intensity inversions between the stoichiometric model and the experimental one. Peak 1, centered around 2 Å, represents all metal–oxygen bonding distances; the low atomic scattering factor of oxygen explains why this peak is weak even if this distance is the most frequent in the cell. The second peak at 2.97 Å is the octahedral–octahedral site distance, while the third indicates the tetrahedral–tetrahedral (3.48 Å) and tetrahedral–octahedral (3.63 Å) site distances.[3] Beyond these three, reduced RDF peaks cannot be analysed simply as unique distance contribution. Thus the low intensity of the third peak in the experimental reduced RDF would be due to a lower content of metal in tetrahedral sites than in octahedral sites. Model c is relative to a nonstoichiometric model of $NiMn_2\square_{3\delta/4}O_{4+\delta}$ where vacancies are present in octahedral and tetrahedral sites, whereas model d represents the same composition but with 100% of vacancies in tetrahedral sites. Clearly model d better fits the experimental reduced RDF of MN573.

In a second step we attempted to reach the best fit of the experimental reduced RDF by a model carefully adjusted manually step by step. The best result was obtained for a 100% tetrahedral vacancy model with structural parameters summed up in Fig. 4. Thermal parameters (b) were adjusted to fit perfectly the second and the third peak of the reduced RDF. However, in that case, the peaks for longer distances are systematically overevaluated in the model. This behavior is particularly visible in the 7–12 Å range. This is a direct cause of the amorphous nature of MN573. Indeed, our model is a purely crystallographic one. Thermal parameters are the same for short distance interaction as for long distance interaction. The reduced length of coherence due to the amorphous nature of MN573 causes a peak broadening of the experimental reduced RDF for long distance interactions. This effect was not taken into account by the model. After 12 Å the overvaluation of peak intensities in the theoretical reduced RDF decreases because an eight-unit cell model is not big enough to represent completely MN573, where grain size is surely bigger than eight unit cells. Long range interaction numbers are thus underestimated in the model, but an eight-unit cell model is the maximum for our computing possibilities. With these remarks taken into account, the goodness of fit is excellent and the estimation of vacancies localization and content is certainly good. However, the cationic distributions of manganese and nickel have a negligible effect because the

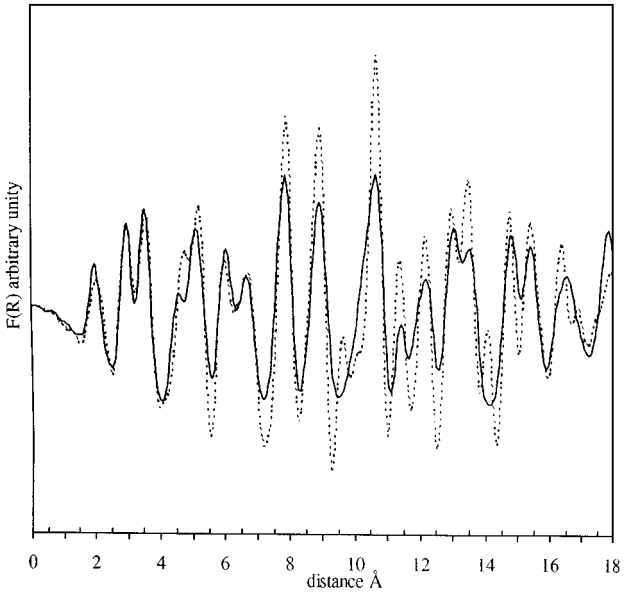

FIG. 4. Experimental and calculated reduced RDF for MN573. Spinel model: $Ni^{2+}_{0.35}\square_{0.65}[Ni^{2+}_{0.27}Ni^{3+}_{0.16}Mn^{4+}_{1.57}]O_4$ ($a = 8.29$ Å, UO = 0.385, bO = 0.0025 Å^2, bNi and bMn = 0.002 Å^2).

[3] Those distances are given for a cubic spinel structure with $a = 8.40$ Å.

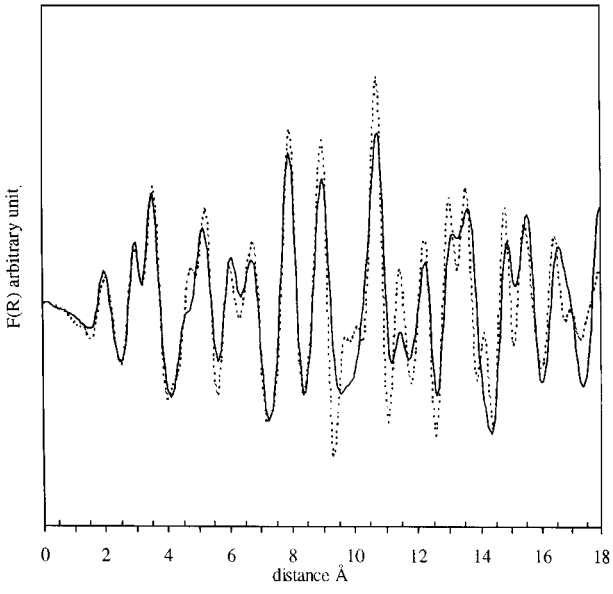

FIG. 5. Experimental and calculated reduced RDF for MN623. Spinel model: $Ni^{2+}_{0.55}\square_{0.45}[Ni^{2+}_{0.3}Mn^{3+}_{0.5}Mn^{4+}_{1.2}]O_4$ ($a = 8.31$ Å, UO = 0.388, bO = 0.0025 Å^2, bNi and bMn = 0.002 Å^2).

scattering factors of nickel and manganese are too similar to cause appreciable discrepancies on the reduced RDF.

Figure 5 shows the same kind of work which has been done on MN623 (decomposed at 623 K). The best model fitting was obtained also for a 100% tetrahedral vacancy hypothesis but with less vacancy. Because this compound is better crystallized, the statistical disorder is lower and the experimental reduced RDF peak broadening in the long distances range is smaller.

DISCUSSION

The WAXS study confirms the ATG study: thermal decomposition of mixed manganese–nickel oxalate in air at low temperature leads to mixed spinel oxides with a high content of vacancies. Moreover, WAXS study shows that these vacancies are essentially located in tetrahedral sites. The proportion of nonstoichiometry obtained from both studies is almost the same for MN623 oxide ($\delta = 0.7$), but the value obtained for MN573 from WAXS is somewhat higher ($\delta = 1.1$) than those from TGA analysis ($\delta = 0.85$).

We examine here how Mn and Ni cations are distributed into the spinel sites. The high content of vacancies imposes a high valency state for the cations. Then we assume there are no more Mn^{2+} cations. On the other hand, among the Ni^{2+}, Mn^{3+}, and Mn^{4+} cations, Ni^{2+} probably has the least octahedral preference (17). Hence the cation distribution for MN623 would be

$$Ni^{2+}_a\square_{0.45}[Ni^{2+}_b Mn^{3+}_c Mn^{4+}_d]O_4^{2-}. \quad [12]$$

The four coefficients a, b, c, and d can be calculated by resolving the system of the four equations

$$\text{Sum of } T_d \text{ sites} = 1 \Rightarrow a + 0.45 = 1 \quad [13]$$

$$\text{Sum of } O_h \text{ sites} = 2 \Rightarrow b + c + d = 2 \quad [14]$$

$$\text{Mn} = 2 \times \text{Ni} \Rightarrow c + d = 2(a + b) \quad [15]$$

$$\text{Electrical neutrality} \Rightarrow 2a + 2b + 3c + 4d = 8. \quad [16]$$

We found $a = 0.55$, $b = 0.3$, $c = 0.5$, and $d = 1.2$, which lead to the distribution

$$Ni^{2+}_{0.55}\square_{0.45}[Ni^{2+}_{0.3}Mn^{3+}_{0.5}Mn^{4+}_{1.2}]O_4^{2-}. \quad [17]$$

For MN573, taking $\delta = 0.85$, we obtain in a similar way

$$Ni^{2+}_{0.47}\square_{0.53}[Ni^{2+}_{0.35}Mn^{3+}_{0.24}Mn^{4+}_{1.41}]O_4^{2-}. \quad [18]$$

Now if we take $\delta = 1.1$, it becomes impossible to write a distribution such as

$$Ni^{2+}_{0.35}\square_{0.65}[Ni^{2+}_b Mn^{3+}_c Mn^{4+}_d]O_4^{2-}. \quad [19]$$

because even if all the manganese cations were Mn^{4+} ($c = 0$), the mean valency mv of the nickel cations would be

$$(3 - 0.65)\tfrac{2}{3}4 + (3 - 0.65)\tfrac{1}{3}\text{mv} = 8 \quad [20]$$

from which we find mv = 2.2. This would imply that a part of the nickel cations are in the Ni^{3+} state, which leads to the distribution

$$Ni^{2+}_{0.35}\square_{0.65}[Ni^{2+}_{0.27}Ni^{3+}_{0.16}Mn^{4+}_{1.57}]O_4^{2-}. \quad [21]$$

A study by XPS, at the present time under development, confirms the presence of Ni^{3+} in these oxides. Hence, the last distribution appears to be probably the best.

CONCLUSION

The WAXS study on low temperature decomposed mixed oxalates proves that, in the amorphous state, the structural arrangement of manganese, nickel, and oxygen atoms undoubtedly follows a spinel structure. The oxalate decomposition probably leads directly to a spinel structure with a very high content of vacancies localized by an overwhelming majority in tetrahedral sites. Thermogravimetric analyses confirm that these oxides have a great nonstoichiometry proportion; the highest value ($\delta \approx 0.9$) is noticed for the compound synthesized at 573 K.

SUPPLEMENTARY MATERIAL AVAILABLE

A complete description of the WAXS data treatment is available as supplementary material.

REFERENCES

1. E. Jabry, G. Boissier, A. Rousset, R. Carnet, and A. Lagrange, *J. Phys. Colloq.* **47,** 843 (1986).
2. B. Gillot, J. L. Baudour, F. Bouree, R. Metz, R. Legros, and A. Rousset, *Solid State Ionics* **58,** 155 (1992).
3. X. X. Tang, A. Manthiram, and J. B. Goodenough, *J. Less-Common Met.* **156,** 357 (1989).
4. A. Feltz and J. Topfer, *Z. Anorg. Allg. Chem.* **576,** 71 (1989).
5. J. Topfer and J. Jung, *Thermochim. Acta.* **202,** 281 (1992).
6. C. Laberty, P. Alphonse, J. J. Demai, C. Sarda, and A. Rousset, *Mater. Sci. Bull.*, in press.
7. E. Jabry, G. Boissier, A. Rousset, P. Carnet, and A. Lagrange, *in* "Science of Ceramics 13" (P. Odier, F. Cabannes, and B. Calos, Eds.), p. 843. *J. Phys. C1*, 1986.
8. R. Legros, R. Metz, and A. Rousset, *J. Mater. Sci.* **25,** 4410 (1990).
9. A. Rousset, R. Legros, and A. Lagrange, *J. Eur. Ceram. Soc.* **13,** 185 (1994).
10. J. L. Baudour, F. Bouree, M. M. A. Fremy, R. Legros, A. Rousset, and B. Gillot, *Physica B* **180,** 97 (1992).
11. T. Vogt, C. Faulmann, R. Soules, P. Lecante, A. Mosset, P. Castan, P. Cassoux, and J. Galy, *J. Am. Chem. Soc.* **110,** No. 6, 1833 (1988).
12. P. Lecante, A. Mosset, and J. Galy, *J. Mater. Sci.* **27,** 3286 (1992).
13. H. Schneider, D. Voll, B. Saruhan, J. Sanz, G. Schrader, C. Ruscher, and A. Mosset, *J. Noncryst. Solids* **178,** 262 (1994).
14. M. Norman, *Acta Crystallogr.* **10,** 370 (1957); J. Krogh-Moe, *Acta Crystallogr.* **9,** 951 (1956).
15. D. T. Cromer and J. T. Waber, "International Tables for X-ray Crystallography," Vol. 4. Kynoch Press, Birmingham, 1974.
16. P. Debye, *Ann. Phys.* (*Leipzig*) **46,** 809 (1915).
17. A. Navrotsky and O. J. Kleppa, *J. Inorg. Nucl. Chem.* **29,** 2701 (1967).